Macroscopic rate equation modeling of trapping/detrapping of hydrogen isotopes in tungsten materials

E.A. Hodille [a], *, X. Bonnin [b, 1], R. Bisson [c], T. Angot [c], C.S. Becquart [d], J.M. Layet [c], C. Grisolia [a]

[a] CEA, IRFM, F-13108 Saint Paul lez Durance, France
[b] LSPM-CNRS, Université Paris 13, Sorbonne Paris Cité, F-93430 Villetaneuse, France
[c] Aix-Marseille Université, PIIM, CNRS, UMR 7345, 13397 Marseille, France
[d] Université Lille I, UMET, UMR 8207, 59655 Villeneuve d'Ascq cédex France

HIGHLIGHTS

- Code development to solve numerically the model equations of diffusion and trapping of hydrogen in metals.
- Parametrization of the model trapping parameters (detrapping energies and density): fitting of experimental TDS spectrum.
- Confrontation model/experiment: evolution of retention with fluence and implantation temperature.
- Investigation of period of rest between implantation and TDS on retention and depth profile.

ARTICLE INFO

ABSTRACT

Relevant parameters for trapping of Hydrogen Isotopes (HIs) in polycrystalline tungsten are determined with the MHIMS code (Migration of Hydrogen Isotopes in MaterialS) which is used to reproduce Thermal Desorption Spectrometry experiments. Three types of traps are found: two intrinsic traps (detrapping energy of 0.87 eV and 1.00 eV) and one extrinsic trap created by ion irradiation (detrapping energy of 1.50 eV). Then MHIMS is used to simulate HIs retention at different fluences and different implantation temperatures. Simulation results agree well with experimental data. It is shown that at 300 K the retention is limited by diffusion in the bulk. For implantation temperatures above 500 K, the retention is limited by trap creation processes. Above 600 K, the retention drops by two orders of magnitude as compared to the retention at 300 K. With the determined detrapping energies, HIs outgassing at room temperature is predicted. After ions implantation at 300 K, 45% of the initial retention is lost to vacuum in 300 000 s while during this time the remaining trapped HIs diffuse twice as deep into the bulk.

© 2015 Elsevier B.V. All rights reserved.

1. Introduction

Tungsten (W) is a serious candidate material for plasma facing components (PFC) in fusion devices such as ITER and DEMO thanks to its thermal properties. Due to plasma/wall interaction, W-based PFC will be subject to high particle fluxes (10^{20}–10^{24} m²/s) of hydrogen isotopes (HIs). Fuel particles implanted in the subsurface region of PFC could diffuse into the tungsten matrix and be trapped deeper in the bulk. It causes safety issues because of the regulation-limited amount of tritium in the vessel walls as well as operation concerns due to possible uncontrolled HIs recycling fluxes that can affect global plasma stability. So, migration and trapping of deuterium have been extensively studied; see for instance reviews by Causey [1], Skinner et al. [2] and Tanabe [3].

The development of a global tokamak wall model interacting with hydrogen isotopes by taking into account all the physical processes (particles implantation, migration, trapping, outgassing …) is necessary in order to extrapolate the fuel retention in W-based plasma facing materials for ITER. In this approach, macroscopic rate equations (MRE) models are an efficient way to

investigate migration and trapping of HIs in metallic materials from nanometers to centimeters scales. The rate equation model for hydrogen diffusion including hydrogen trapping in materials was originally discussed by McNabb et al. [4] and used for a number of metals such as steel [5,6] and tungsten [7–11].

In the present work, a code based on a rate equations model has been developed to deal with the trapping of HIs in W. It is named MHIMS (Migration of Hydrogen Isotopes in MaterialS) [12] and it can be seen as a light version of the HIIPC models developed by Sang et al. [13] for tokamaks inventory simulations. In addition to the reasonable computational resources necessary for running MHIMS, we will detail here how MHIMS is a good tool to extract, from laboratory experiments, fundamental parameters of the HIs—tungsten interaction and how it can be used for experimentally relevant predictions. MHIMS is able to model particles implantation with traps creation during plasma wall interaction, particles depth profiles evolution in the material and Thermal Desorption Spectrometry (TDS) measurements. In the first part of this paper, the equations of the model are described (Section 2). Then, simulation results are benchmarked against well controlled laboratory experiments from the literature performed with polycrystalline tungsten samples that we consider as a reference case (Section 3). Using this benchmarked set of parameters, we compare MHIMS simulations of the evolution of the retention as a function of fluence and implantation temperature with a larger set of laboratory experiments. The objective of this part of our work is to test the robustness of our model and its predictive ability (section IV). Finally, predictions on deuterium outgassing at room temperature are made and their influences on the interpretation of laboratory experiments are discussed (Section 5).

2. Description of MHIMS model

An earlier introduction to our model can be found in Refs. [12], but we provide here a more comprehensive and updated account. Fig. 1 presents the general energy diagram of a hydrogen atom inside a metal with two types of trapping sites present in the bulk of the material. $E_R + E_S$ is the energy barrier of the hydrogen atom penetration into the metal matrix. E_R is the energy barrier for the H atom to overcome in order to reach the surface (a preliminary step for surface recombination). E_D is the barrier of diffusion of H in the metal matrix through solute sites. $E_{B,1}$ and $E_{B,2}$ are binding energies of HIs located in two different trap types present in the metal. Thus, energy barriers to come out of these traps, called detrapping energies, are respectively $E_{T,1} = E_{B,1} + E_D$ and $E_{T,2} = E_{B,2} + E_D$.

In our MRE model, HIs are split into two populations: mobile (or solute) and trapped species. C_m stands for the concentration of mobile particles and $C_{t,i}$ for the concentration of trapped particles in the ith trap type. In the following, the concentrations will be normalized to the metal density i.e. they are expressed in atomic fraction (at.fr.).

The temporal variation of each population is described by Equations (1) and (2).

$$\frac{\partial C_{t,i}}{\partial t} = -S_{trap,i \to mobile} + S_{mobile \to trap,i} \tag{1}$$

$$\frac{\partial C_m}{\partial t} = D(T) \cdot \frac{\partial^2 C_m}{\partial x^2} - \sum \frac{\partial C_{t,i}}{\partial t} + S_{ext} \tag{2}$$

where $S_{mobile \to trap,i}$ is the source of mobile particles being trapped, $S_{trap,i \to mobile}$ corresponds to trapped particle being detrapped and S_{ext} is the exterior source of particles entering the volume. $D(T) = D_0 \cdot e^{-\frac{E_D}{k \cdot T}}$ is the diffusion coefficient of HIs in the metal matrix (in m² s⁻¹) with the energy barrier E_D represented in Fig. 1 (k is the Boltzmann constant). Dealing with HIs, the diffusion coefficient has to be mass dependent, thus as in Refs. [10,11] we used $D_{HI} = \frac{D_H}{\sqrt{HI\ atomic\ mass}}$ for the diffusion of any Hydrogen Isotope. As a remark, if an equilibrium is considered between trapped and solute particle, the model correspond to Oriani's one [5] which envisaged the HIs trapping and migration as an apparent diffusion from trap to trap: in such model, the retention variation with fluence would vary as fluence^0.5 (i.e. limited by diffusion).

For each trap type, there are a finite number of available traps. We also assume that each trap captures only one HI atom. The trap density is noted n_i and it can evolve with space (inhomogeneous spatial distribution) and with time, since we include trap creation in this model (see further in the text) in contrast to some previous MRE models [7,10,11]. The number of solute sites is fixed. We call n_{solute} the number of solute sites per tungsten atoms and it is considered that $n_{solute} \gg \sum n_i$. Therefore we consider that for each trap, its first neighbor is a $i$solute site. It is also considered that the solute concentration is low: $C_m \ll n_{solute}$ which means that for each trapped particle, there is a free neighbor solute site which permits detrapping. Following these assumptions, $S_{mobile \to trap,i}$ and $S_{trap,i \to mobile}$ can be expressed as follows [8]:

$$S_{trap,i \to mobile} = \frac{1}{\tau_a} \cdot C_{t,i} \tag{4}$$

$$S_{mobile \to trap,i} = \frac{1}{\tau_b} \cdot \frac{C_m}{n_{solute}} \cdot (n_i - C_{t,i}) \tag{5}$$

Here, τ_a and τ_b are time constants for respectively the detrapping and trapping processes. As in Refs. [7,10,11], the detrapping time constant τ_a can be expressed as a frequency term. Using the energy barrier $E_{T,i} = E_D + E_{B,i}$ of Fig. 1, $\frac{1}{\tau_a} = \nu_0 \cdot e^{-\frac{E_{T,i}}{k \cdot T}}$ and Equation (4) becomes:

$$S_{trap,i \to mobile} = \nu_0 \cdot C_{t,i} \cdot e^{-\frac{E_{T,i}}{k \cdot T}} \tag{6}$$

where ν_0 is the pre-exponential factor (or attempt frequency) in s⁻¹. It is important to specify the value of ν_0 when this set of equations is
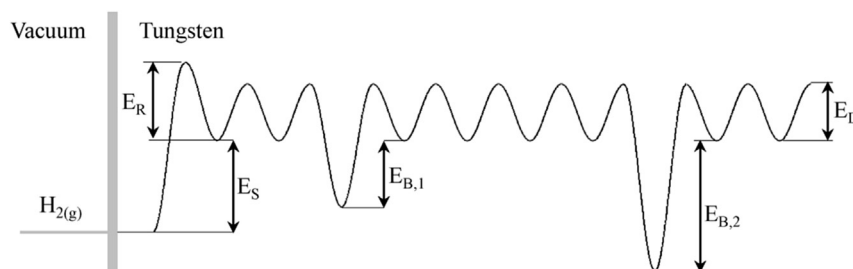

Fig. 1. Potential energy diagram for a hydrogen atom in tungsten.

used to fit TDS experiments. Indeed, for a same detrapping energy, the simulated peak can be shifted by about 35 K if ν_0 changes only by an order of magnitude. In the following, ν_0 is taken equal to 10^{13} s^{-1} accordingly with [7,10]. In Refs. [8,9], ν_0 is expressed as a function of the lattice constant and of the diffusion coefficient and $\nu_0 \sim 3 \times 10^{13}$ s^{-1} for hydrogen and $\nu_0 \sim 2 \times 10^{13}$ s^{-1} for deuterium which is of the same order of magnitude. The trapping source can also be understood as a detrapping effect, where the HI atom detraps from a solute site before falling in a trap site of type i. The trapping attempt frequency $1/\tau_b$ is usually expressed as a function of the diffusion coefficient by $\tau_b = \lambda^2 / D(T)$, where λ is the distance between 2 solute sites or between a solute and a trap site. So the trapping source term (5) becomes:

$$S_{mobile \to trap,i} = \frac{D(T) \cdot n_i}{\lambda^2 \cdot n_{solute}} \cdot C_m \cdot \left(1 - \frac{C_{t,i}}{n_i}\right) \quad (7)$$

and n_{solute}/n_i is the average number of solute sites between two trap sites.

The exterior source of particles S_{ext} is present only if a flux of ions is interacting with the materials (plasma or ion beam exposure). The flux φ of energetic ions is implanted at a certain depth following a distribution law $f(x)$ that is modeled using SRIM [15] and which depends on the implantation energy of ions. This depth implantation distribution $f(x)$ is approximated with a Gaussian function in our model. Non-implanted ions are those which are reflected: the reflection coefficient r is also calculated with SRIM and we use it to define the exterior source of HIs:

$$S_{ext} = (1 - r) \cdot \varphi \cdot f(x) \quad (8)$$

When all the particle sources expressions of Equations (6)–(8) are inserted in Equations (1) and (2) for the temporal evolution of HIs populations, we obtain the following set of equations which are solved numerically:

$$\frac{\partial C_{t,i}}{\partial t} = -\nu_0 \cdot C_{t,i} \cdot e^{-\frac{E_{T,i}}{k \cdot T}} + \frac{D(T) \cdot n_i}{\lambda^2 \cdot n_{solute}} \cdot C_m \cdot \left(1 - \frac{C_{t,i}}{n_i}\right) \quad (9)$$

$$\frac{\partial C_m}{\partial t} = D(T) \cdot \frac{\partial^2 C_m}{\partial x^2} - \sum \frac{\partial C_{t,i}}{\partial t} + (1 - r) \cdot \varphi \cdot f(x) \quad (10)$$

The diffusion coefficient $D(T)$ of HIs in tungsten has been measured by Frauenfelder [14] for hydrogen: $4.1 \times 10^{-7} \cdot e^{-\frac{0.39eV}{k \cdot T}}$ $(m^2 \cdot s^{-1})$. This value is in agreement with other experimental data as shown in several review papers [1–3] and has been rationalized with theoretical calculations [16–18]. We therefore take the experimental value to parameterize our model. Tungsten crystallizes with a bcc lattice. It has been shown by *ab initio* calculations [16] that hydrogen diffuses between tetrahedral interstitial sites. Thus, $\lambda = \frac{a_W}{2 \cdot \sqrt{2}} \sim 110$ pm with a_W the lattice constant of tungsten equal to 316 pm and $n_{solute} = 6$ since there are 12 tetrahedral sites and 2 tungsten atoms in the bcc lattice.

As suggested on the left side of Fig. 1, there can be potentially a recombination barrier for atoms at the surface of the metal since they escape in the vacuum mostly in the form of HI molecules. Nevertheless, experimental measurements of HI retention in tungsten strongly suggest that desorption of HIs from the surface is far from being the rate limiting step [1,19]. So, we consider that the boundary condition is a Dirichlet boundary condition [10]: $C_m(x = 0, t) = 0$.

We will now turn back to the time evolution of the total trap density $\sum_i n_i$. In the work of Haasz and coworkers [20], the deuterium retention dependency on the deuterium ion incident

flux has been studied. It was observed that the retained fraction of impinging deuterium ions was low and flux dependent until a flux threshold of 10^{18} D·m^{-2}·s^{-1} above which it became high and flux independent (for flux up to 5×10^{19} D/m²/s). Subsequently, the analysis of the evolution of the deuterium depth profile as a function of fluence [21,22] showed that deuterium concentration is inhomogeneous throughout the bulk and can be divided in three zones. The highest HIs concentration is found in the ion stopping range, then a decreasing tail of high HIs concentration is measured in the first μm depth and finally a HIs low concentration plateau is found. While the latter zone is related to natural (intrinsic) defects in the material, the two former high concentration zones were shown to increase much faster than expected from the increase of fluence. These observations were explained by ion-induced trap creation through two different processes [22]. The first trap creation process is operative in the ion stopping zone. It could be due to trap creation through local supersaturation of HIs in the ion stopping range (i.e. solute/mobile concentrations exceeding the solubility limit), subsequently inducing stresses in the material and creating extended defects such as vacancy clusters and bubbles [9,22,24]. The second trap creation process occurring in the first μm results from the diffusion of the HIs located in the implantation zone and being "pushed" toward the bulk by the local stress field. The resulting increase of HIs concentration could also lead to the plastic deformation of the tungsten matrix from deuterium supersaturation [20,21,23].

In our model these two processes are taken into account through a time variation of the density of created traps n_3 expressed as:

$$\begin{aligned}
\frac{dn_3}{dt} = (1 - r) \cdot \varphi \cdot &\left[\left(1 - \frac{n_3}{n_{3amax}}\right) \cdot \eta_{3a} \cdot f(x) \right. \\
&+ \left. \left(1 - \frac{n_3}{n_{3bmax}}\right) \cdot \eta_{3b} \cdot \theta_{x_p}(x)\right]
\end{aligned} \quad (11)$$

where both traps creation rates are proportional to the implanted flux φ. Thus, for both type of traps, the amount of created traps is proportional to the HIs fluence. In the brackets of Equation (11), the first term corresponds to the traps creation in the stopping zone $f(x)$ and follows the expression proposed by Ogorodnikova et al. [22] based on Duesing et al.'s work [25]. In this zone, the traps density is limited to n_{3amax} and the creation rate η_{3a} is the number of traps created per implanted ion. The second term in the brackets of Equation (11) corresponds to traps creation in the first μm of the material. This expression was not included in previous models. The form of the expression of the second trap creation process resembles the one of the first trap creation process but with a different depth distribution. We chose an empirical depth distribution for these traps with the simple form $\theta_{xp}(x) = 1/x_p$ between 0 and x_p, 0 elsewhere and $x_p \sim 1$–3 μm [21]. This second type of created traps is density limited to n_{3bmax} and the creation rate is η_{3b}. In addition, to agree with the observed flux dependence by Haasz and coworkers [20], a threshold of trapping creation process is implemented: only if $\varphi > 10^{18}$ D.m^{-2}.s^{-1}, does traps creation take place.

Firstly, we note that the first term in the brackets of Equation (11) could also account for trap creations through inelastic collisions of incident impurities with W atoms. However, in the set of experiments we chose to simulate the amount of impurities in the beam was carefully controlled thus we neglect this contribution. Secondly, the choice of the empirical depth distribution for the second term in Equation (11) is based on its resemblance with the erfc() functional form obtained from non-steady-state diffusion. It however behaves with a steeper decay that could render the non-

linear effects related to the super-saturation process. A more exact functional form should account for the intertwined influence from the incident flux and the material temperature that define the diffusion rate toward the bulk as well as the concentration in the implantation zone. In such, this is an extended theoretical study that would necessitate further experimental data for validation and thus it is out of the scope of this article. Nevertheless, Ogorodnikova et al. have shown [26] that the two HI concentration distribution components remain for deuterium implantation at 320 K and 500 K. Therefore Equation (11) should render at least qualitatively the evolution of HIs concentration in the bulk of the material even at temperature higher than 300 K. Thirdly, our choice of a fluence dependent model is guided by our goal to simulate experiments which were performed with fluxes comprised between 10^{19} and 10^{20} D/m^2/s and fluence between $10^{21} - 10^{24}$ D/m^2. Indeed, Haasz and coworkers observed a HIs retention which is independent of the flux in the range $10^{18} - 10^{19}$ D/(m^{2}s) for the fluence range $10^{21} - 10^{23}$ D/m^2. It suggests that the integrated amount of trap created is in this range independent to the flux and only dependent on the fluence. One may note that Lindig et al. [24] found a change in surface morphology related to a change of flux, so $n_{max}$and η_{max} may also depend on the flux. However, this was observed for higher fluxes ($10^{21} - 10^{22}$ D/(m^{2}s)) and at higher fluence (10^{26} D/m^2) than for the works of Ogorodnikova *et al.*[9,22] and Haasz and coworkers [20,27–29] we want to simulate in the present article.

Finally, we emphasize that MHIMS is designed to simulate a typical implantation − TDS retention measurement experiment by considering 3 different phases:

- The implantation period, lasting $t_{implantation}(s)$ at a sample temperature T_{imp} (K),
- The resting period between the end of the implantation and the beginning of the retention measurement. Here the samples are maintained at constant temperature $T_r(K)$ for a period lasting $t_{rest}(s)$, the resting time,
- The TDS phase during which the temperature is increased with a given heating ramp $\beta(expressed\ in$ K s$^{-1})$.

MHIMS will be used to simulate laboratory experiments and to this end we will use published experimental parameters representative for these 3 phases. It will only deal with results obtained with polycrystalline samples.

3. MHIMS benchmarking on laboratory experiments

MHIMS is used in Ref. [12] to catch critical parameters from TDS experiments and used it in HIIPC to simulated trapping/migration/desorption of HIs during real tokamak material thermal cycle. In this section, we come back to this simulation in order to explain in more detail the results shown in Ref. [12]. We used laboratory experiments with hot-rolled W from Ogorodnikova et al. [9] since these data were obtained with an all *in-situ* apparatus, i.e. there was no air exposure between deuterium implantation and retention measurements with TDS. In their article, Ogorodnikova et al. simulate the TDS measurements for a fluence of 10^{22} D m^{-2} with a rate equations model consisting of 2 detrapping energies related to: an intrinsic trap (0.85 eV) and an extrinsic trap (1.45 eV) i.e. a trap created during deuterium ions implantation. We also fit this TDS measurement, simulating implantation at a flux of 2.5×10^{19} D/m^2/s with 200 eV/D ions (r = 0.56), a resting time of 50 s and a heating ramp up of 8 K/s [9]. Their experimental data and their model adjustment are shown in Fig. 2 (a) together with our MHIMS simulation. We present also the deuterium depth profile just after the resting time (i.e. before the TDS heating ramp begins) determined by MHIMS in Fig. 2(b). For the MHIMS simulation, three traps have been used:

- trap 1: a low energy intrinsic trap: $E_1 = 0.87$ eV, $n_1 = 1 \times 10^{-3}$
- trap 2: a medium energy intrinsic trap: $E_2 = 1.00$ eV, $n_2 = 4 \times 10^{-4}$
- trap 3: a high energy extrinsic trap: $E_3 = 1.50$ eV with the following density of induced trap:
  ○ $n_3 = n_{3a} + n_{3b}$
  ○ $n_{3a}(t = 0s) = n_{3b}(t = 0s) = 0$
  ○ $n_{3amax} = 1 \times 10^{-1}$, $\eta_{3a} = 6 \times 10^{-4}$
  ○ $n_{3bmax} = 1 \times 10^{-2}$, $\eta_{3b} = 2 \times 10^{-4}$, $x_p = 1$ μm.

The values of these traps densities fulfill the condition $n_{solute} > > n_i$. In addition, the concentration of mobile particles is calculated to be ~1×10^{-7}, the condition $C_m < < n_{solute}$ is also fulfilled.

The simulated TDS measurement given by MHIMS reproduces well both the position and the shape of the experimental TDS spectra, the relative error of the integral of each spectra being less than 10%, and they do not miss the evident broad aspect of desorption peaks of deuterium in contrary to Ogorodnikova et al.'s original fit. Note that the detrapping energies of trap 1 and trap 3 in MHIMS agree well with Ogorodnikova et al. detrapping energies [9]. At first glance, the addition of a second intrinsic trap to better reproduce the experimental data of Ogorodnikova et al. may look artificial. However, intrinsic traps are usually associated with dislocations, grain boundaries and/or vacancies [9,22] which are all present in tungsten polycrystals. To these 3 types of defects could correspond at least two different binding energies, as it has been shown recently by Xiao and Geng [30]. Furthermore, *ab-initio* calculations have recently demonstrated that multiple hydrogen atoms can be trapped around a single defect, leading to a distribution of binding energies [18,31,32]. These theoretical predictions justify our use of more than a single intrinsic trap.

In a MHIMS simulation (fluence = 10^{22} D/m^2), we have access to the evolution of the deuterium density profile in the bulk of the material which allows for a better understanding of experimental observables such as a TDS peak. For example in Fig. 5 of the article of Ogorodnikova et al. [9] one can see that TDS peaks shift to higher temperature as fluence is increased from 10^{22} to 10^{23} D.m^{-2}. This TDS peak behavior is well reproduced in our simulation (not shown) and can be rationalized as being due to particles trapping deeper in the tungsten bulk (Fig. 2(b)), since to a higher fluence corresponds a longer implantation at constant flux and thus a longer time for particles diffusion into the bulk. This difference in deuterium density profile shows up in TDS experiments as a delay of peak appearance i.e. the TDS peak appears shifted to higher temperature. Besides, looking at the bulk part of the depth profile (Fig. 2(b)), it can be seen that the deuterium concentration approaches the traps density. The concentration of trapped particles depends on a balance between Equations (6) and (7). Therefore, at a given temperature, it mainly depends on the couple (ν_0, $E_{T,i}$) and the presence of mobile particles near a trap. With a large flux like the one used here, the source of mobile particles is sufficient to saturate both traps 1 and 2. The traps creation in the stopping zone can be seen in the zoom of the sub-surface part. The density of created trap in the area reaches 2×10^{-2} trap/W for a fluence of 10^{22} D m^{-2} and 10^{-1} trap/W (= n_{3amax} = maximum density) for a fluence of 10^{23} D m^{-2} which is very high. It is probable that in this zone W is deeply damaged. The other population of created traps (until 1 μm) is not visible for fluence of 10^{22} D m^{-2} and appears only at higher fluences (10^{23} D m^{-2}). However, the influence of these created traps is seen in the simulated TDS spectrum: they are at the origin of the tail at high temperature observed between 650 and 700 K. In this study, the traps created up to 1 μm are associated with a high detrapping
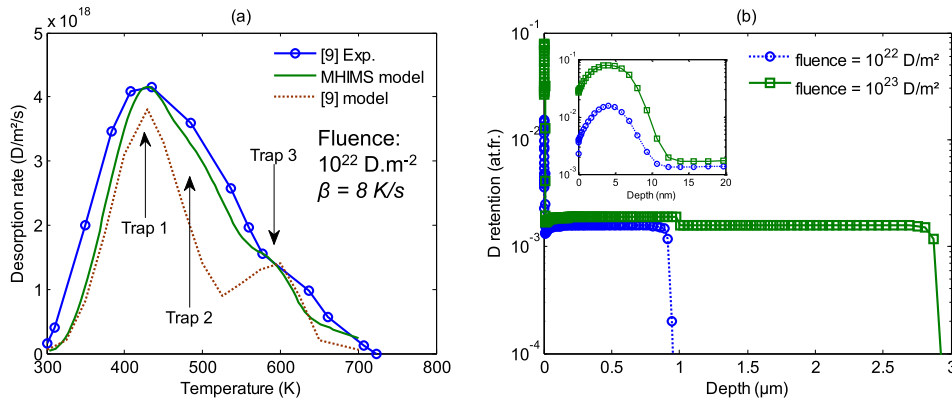
Fig. 2. (a) MHIMS simulated TDS spectrum compared with experimental and model results of Ogorodnikova et al. [9]. (b) MHIMS simulated depth profile of deuterium just before the beginning of the TDS measurement for 2 fluences (10^{22} and 10^{23} D m^{-2}). Implantation simulated at a flux of 2.5×10^{19} D/m^2/s with 200 eV/D ions, resting time is 50 s, the heating ramp rate is 8 K/s.
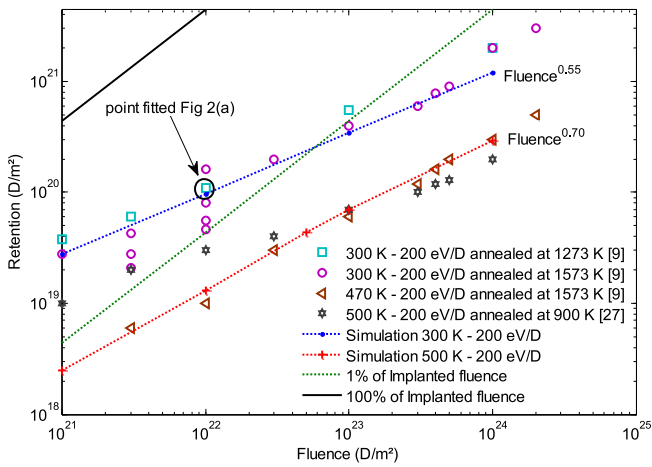

Fig. 3. Evolution of deuterium retention vs 200 eV/D ions fluence. Experimental data for 300 K–470 K [9] and 500 K [30]. Simulated results for 300 K and 500 K "Fitted point" stands for the MHIMS simulation of Fig. 2(a) used to calibrate the code. Implantation simulated at a flux of 2.5×10^{19} D/m^2/s with 200 eV/D ions, resting time is 50 s.
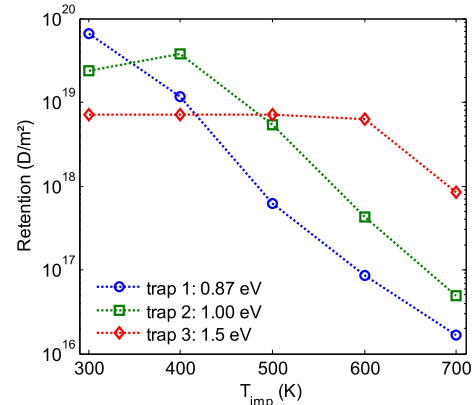

Fig. 5. Evolution of retention in each trap in function of implantation temperature. Implantation simulated at a flux of 2.5×10^{19} D/m^2/s with 200 eV/D ions, resting time is 50 s.

energy but in Ref. [22] they are associated to low detrapping energy. The association is ambiguous due to difficulties in understanding correctly what happens during trap creation. Further experimental studies are needed to understand properly these processes. However, the retention in these created traps does not influence the observations, the discussion and the conclusion in the following.
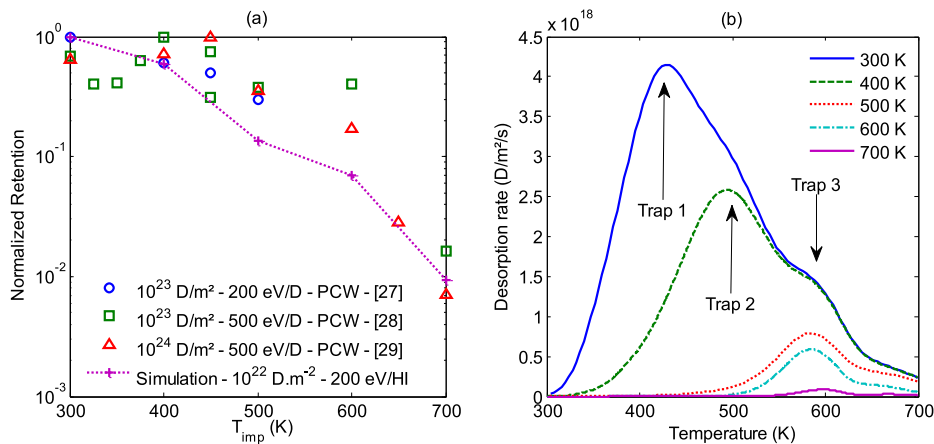

Fig. 4. (a) Evolution of (normalized) deuterium retention as a function of implantation temperature. Crosses: MHIMS simulations. Other symbols: experimental data. (b) MHIMS simulation of TDS measurements for different implantation temperature between 300 K and 700 K. Implantation simulated at a flux of 2.5×10^{19} D/m^2/s with 200 eV/D ions, resting time is 50 s, the heating ramp up is 8 K/s.

4. Comparison of the MHIMS model with various laboratory experiments

4.1. Variation of retention vs fluence

To test the reliability of the trapping parameters used above, the evolution of retention with fluence at two different implantation temperatures obtained with MHIMS is shown in Fig. 3 together with the experimental data from Ogorodnikova et al. [9] and Tian et al. [27]. Several fluences from 10^{21} to 10^{24} D/m^2 are simulated for implantation temperatures of 300 K and 500 K.

The MHIMS model parameterized on data from Ogorodnikova et al. at 300 K implantation temperature predicts deuterium retention as a function of fluence in excellent agreement with the data of Ogordnikova et al. measured at 300 K and 500 K. Absolute differences are at most of a factor of two. However, when comparing the MHIMS results with the 500 K implantation data of Tian et al. [30] a mismatch by a factor of 5 can be observed at low fluence. This difference is explained by the pre-implantation treatment of the tungsten samples used. The parameters of the model used here have been determined on experiments using a sample pre-annealed at 1273 K during an hour prior to deuterium ion implantation while the data of Tian et al. [27] have been obtained with the sample pre-annealed at 950 K during 30 min. As it is discussed in Refs. [9,12], this pre-annealing has an impact on the intrinsic traps density and so on the overall retention. This is especially visible at low fluences because trap creation is not the dominant retention process. At higher fluences, the difference diminishes because the amount of created traps does not depend on the pre-implantation treatment.

Finally, in Fig. 3, it is observed that the absolute variation of retention with fluence is different for 300 K and 500 K implantations. At 300 K, the retention varies according to the power law fluence$^{0.55}$ while at 500 K, the retention increases as fluence$^{0.7}$. This change in the power law exponent can be interpreted as a transition from diffusion-limited retention (300 K) to trap-creation limited retention (500 K). Indeed for implantation at 500 K, detrapping from the lowest energy intrinsic trap is easy and thus the retention is mainly due to retention in the highest energy intrinsic trap and the extrinsic created trap, i.e. the fraction of retention due to the extrinsic trap increases. Since the extrinsic trap is linearly dependent on the ion flux (within a certain domain, see Eq. (11)), the power exponent for 500 K implantation is closer to unity as compared to 300 K implantation.

4.2. Variation of retention with implantation temperature

The effect of implantation temperatures was simulated in more details by comparison with an extensive set of experimental data from the group of Haasz [27–29] while using the set of parameters benchmarked on Ogorodnikova et al. experiments [9]. In the MHIMS modeling, we used a constant fluence of 10^{22} D/m^2 (limited by calculation time constraints which are temperature dependent) and an ion incident energy of 200 eV/D. Several simulations were made for implantation temperatures from 300 K to 700 K. The experimental data relates to different fluences and implantation energies. To compare the simulation results with experimental data, the retention is normalized over the maximum retention in each data set. The results of our simulations are presented in Fig. 4. Fig. 4(a) shows the same decreasing trends between experiment and simulation with a retention decrease of one order of magnitude for T_{imp} increasing from 300 K to 600 K and then a supplementary retention decrease of another order of magnitude between 600 K and 700 K. The simulated TDS measurements and the differential deuterium retention in each trap type are shown in Figs. 4(b) and 5,

respectively, for all these implantation temperatures. Because trap 1 desorption occurs at ~400 K, the amount of trapped deuterium in trap 1 will decrease rapidly for implantation temperatures above 300 K. Since deuterium detraps efficiently from trap 1 and diffuses into the bulk, it will end up preferably trapped in the highest energy intrinsic trap 2. This explains the relative growth of trap 2 populations as compared to trap 1 between 300 K and 400 K as seen in Fig. 5. From 300 K to 600 K, the population in the extrinsic traps 3 stays nearly constant. It does not significantly increase because trap 3 is created near the implanted zone and when such a trap is created, it is almost immediately filled. Trap 3 population begins to decrease after 600 K as the sample temperature is high enough for detrapping (and thus desorption) to occur from this trap.

Even if the decreasing trends are observed both in experimental data and in simulation results, the normalized retention from experiments seems to be underestimated by the MHIMS simulation. To explain this discrepancy, two effects may be considered.

First, the pre-implantation treatment: authors from Refs. [28,29] use similar annealing as in Ref. [9], which was used here to benchmark the set of parameters of the MHIMS model. So, we can exclude pre-implantation treatment as the reason of the observed difference.

Second, the resting time: Haasz et al. specified that the resting time of their sample is in the 16 h–72 h range [29]. As we will show in the next section, this experimental parameter is the reason for the discrepancy in Fig. 4 between MHIMS simulations and experiments.

5. Effect of the resting time

Studies on deuterium retention in tungsten rarely have considered the influence of the resting time between ion implantation and the retention measurement. One of the reasons is the common assumption that any eventual desorption between implantation and TDS experiment is only due to solute particles. However, with the presence of a low energy trap like the MHIMS lowest energy intrinsic trap (trap 1), there could be significant desorption during a long (hours or more) resting time. To investigate this potential effect, several simulations were realized with different resting times, from 50 s (corresponding to the conditions of Ogordonikova et al. [9]) to 300 000 s (~83 h) i.e. resting times typical of the Haasz group. The implantation was simulated at room temperature (300 K) with incident energy of 200 eV/D and a fluence of 10^{22} D/m^2. After 300 000 s of resting time, also at 300 K, it is seen that 45% of the initial retained particle were lost (Fig. 6(a)).

In Fig. 6(a), the overall deuterium retention and the relative deuterium population in each of the three traps is plotted as a function of resting time, while in Fig. 6(b) is shown the corresponding evolution of the deuterium depth profile. The concomitant decrease, respectively increase, of the deuterium population in trap 1, respectively trap 2 with resting time, shows that deuterium in trap 1 was detrapped and partly retrapped in trap 2. However, the decrease of the deuterium overall retention indicates that part of the deuterium detrapped from trap 1 diffused to the surface and was desorbed in the vacuum. The non-desorbed deuterium population tends to diffuse deeper in the bulk while being trapped in trap 2. After a resting time of 50 s, HIs concentration is saturated in the 1st μm and is almost equal to the initial intrinsic trap concentration i.e. $C_{t,1}(t = 50s) + C_{t,2}(t = 50s) \cong n_1 + n_2 = 1.4 \times 10^{-3}$. After a resting time of 300 000 s, almost all trap 1 sites are empty and the HIs are present up to 1.8 μm: the concentration of HIs is almost equal to $C_{t,1}(t = 300000s) + C_{t,2}(t = 300000s) \cong n_2 = 0.4 \times 10^{-3}$. This result has potentially a profound consequence for the
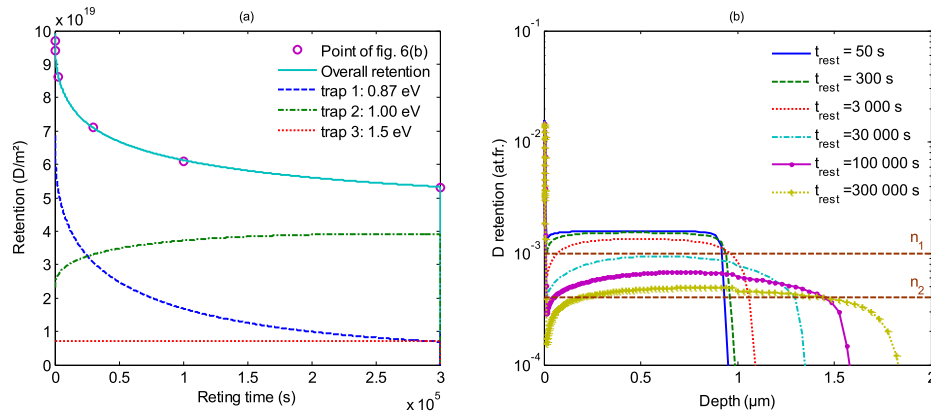
Fig. 6. (a) Evolution of traps population as the resting time is increased (50 s–300 000 s). (b) Deuterium depth profile as a function of resting time. Implantation simulated at a flux of 2.5×10^{19} D/m²/s with 200 eV/D ions.

interpretation of Nuclear Reaction Analysis (NRA) measurements when it is used to extract trap density from deuterium depth profiles: if the resting time between deuterium implantation and NRA measurements is of the order of several tens of hours, then the trapped HI density in low energy intrinsic traps like trap 1 will be strongly underestimated or even not seen. Several tens of hours is actually quite a usual time delay before *ex-situ* NRA measurements. A final remark: the above results are important when deuterium implantation is performed at 300 K. For example, if we model with MHIMS an implantation at 500 K followed by a resting time at 300 K, no desorption during resting time is observed: if trap 1 is not filled during implantation due to high temperature implantation it will not be filled from trap 2 population at 300 K.

As an application of our observation with MHIMS of an effect of the resting time for 300 K implantation, we integrated this resting time parameter in our attempt to reproduce the published data from the group of Haasz [27–29], where the resting time is around 70 h–80 h. The results are shown in Fig. 7. As compared to Fig. 4(a), it is clear that a better agreement between the model and the experimental data is achieved. Thus, it appears that the resting time between the end of ion implantation and the beginning of retention measurements may be an important parameter that any rate equation models should include, as it is the case in MHIMS.
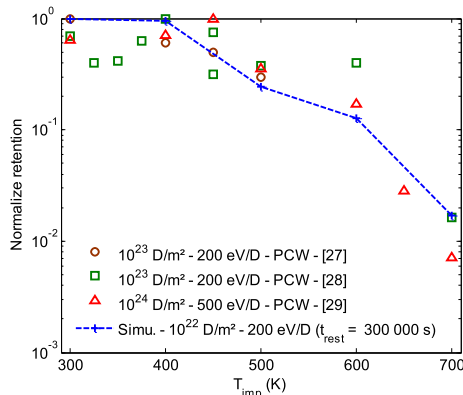
6. Conclusion

MHIMS is a code based on a macroscopic rate equations model including ion-induced trap creation and resting time between the end of ion implantation and the characterization time. It is applied to deal with retention of HIs in tungsten. We use a well-controlled (*in-situ*) TDS experiment from literature to benchmark this model. It is found that HIs can be trapped in three types of trap: two intrinsic traps (detrapping energy 0.87 eV and 1.00 eV) and an extrinsic trap created by ion irradiation (detrapping energy 1.50 eV).

The benchmarked MHIMS code is used to simulate the evolution of retention at difference fluences at 300 K and 500 K. These results are compared to a set of experimental data from different groups. Simulation results are in good agreement with experimental data and quantitative discrepancies are linked to difference in sample preparation. It is observed that for deuterium ions implantation at 300 K, the retention is limited by diffusion in the bulk (trapping in intrinsic trap). On the other hand, for ion implantation at 500 K, retention evolution as a function of fluence is limited by traps creation (extrinsic trap). The evolution of retention with implantation temperature in the 300–700 K range is also well reproduced by the MHIMS model. Similarly to experimental data, it is shown that retention drops by two orders of magnitude with a specific threshold around 600 K. This behavior is rationalized by analysis of the relative deuterium populations in the three types of traps.

Finally, the effect of outgassing at 300 K after ions implantation at 300 K is simulated. After 300 000 s, a loss of 45% of the initial retention is predicted together with an enhanced diffusion in the bulk. Taking into account this outgassing during resting time, the MHIMS model achieves a better agreement with experimental measurements of the implantation temperature dependency of deuterium retention. It is deduced that, if not taken into account, this room temperature outgassing would lead to misinterpretation of NRA data for trap density determination, particularly when a too long resting time is used between implantation at 300 K and NRA measurements.

References

[1] R.A. Causey, J. Nucl. Mater. 300 (2002) 91–117.
[2] C.H. Skinner, A.A. Haasz, V. Kh Alimov, et al., Fusion Sci. Technol. 54 (2008) 891.
[3] T. Tanabe, Phys. Scr. T159 (2014) 014044.
[4] A. McNabb, P.K. Foster, Trans. Metall. Soc. AIME 227 (1963) 618.
[5] R.A. Oriani, Acta Metall. 18 (1970) 147.
[6] A.H.M. Krom, A. Bakker, Metall. Mater. Trans. B 31B (2000) 1475.

Fig. 7. Same as Fig. 4(a) but including in the MHIMS simulation with a 300 000 s resting time. Implantation simulated at a flux of 2.5×10^{19} D/m²/s with 200 eV/D ions.

[7] C. Garcia-Rosales, P. Franzen, H. Planck, et al., J. Nucl. Mater. 233–237 (1996) 803–808.
[8] O.V. Ogorodnikova, Hydrogen and helium recycling at plasma facing materials, NATO Sci. Ser. 54 (2001) 7.
[9] O.V. Ogorodnikova, J. Roth, M. Mayer, J. Nucl. Mater. 313–316 (2003) 469–477.
[10] K. Schmid, V. Rieger, A. Manhard, J. Nucl. Mater. 426 (2012) 247–253.
[11] M. Poon, A.A. Haasz, J.W. Davis, J. Nucl. Mater. 374 (2008) 390–402.
[12] X. Bonnin, et al., J. Nucl. Mater. (2014). http://dx.doi.org/10.1016/j.jnucmat.2014.10.053.
[13] C. Sang, J. Sun, X. Bonnin, et al., Nucl. Fusion 52 (2012) 043003.
[14] R. Frauenfelder, J. Vac. Sci. Technol. 6 (1968) 388.
[15] J.F. Ziegler, M.D. Ziegler, J.P. Biersack, Nucl. Inst. Methods Phys. Res. B 268 (2010) 1818–1823.
[16] K. Heinola, T. Ahlgren, J. Appl. Phys. 107 (2010) 113531.
[17] G.-H. Lu, H.B. Zhou, C. Becquart, Nucl. Fusion 54 (2014) 086001.
[18] N. Fernandez, Y. Ferro, D. Kato, Acta Mater. 94 (2015) 307–318.
[19] R. Bisson, et al., J. Nucl. Mater. (2015) in this theme issue.
[20] M. Poon, R.G. Macaulay-Newcombe, J.W. Davis, et al., J. Nucl. Mater. 307–311 (2002) 723–728.
[21] V. Kh Alimov, J. Roth, M. Mayer, J. Nucl. Mater. 337–339 (2005) 619–623.
[22] O.V. Ogorodnikova, J. Roth, M. Mayer, J. Appl. Phys. 103 (2008) 034902.
[23] J.B. Condon, T. Schober, J. Nucl. Mater. 207 (1993) 1–24.
[24] S. Lindig, M. Balden, V. Kh, Alimov, et al., Phys. Scr. T145 (2011) 014039.
[25] G. Duesing, Cryst. Lattice Defects 1 (1969) 55.
[26] O.V. Ogorodnikova, T. Schwarz-Selinger, K. Sugiyama, et al., J. Appl. Phys. 109 (013309) (2011).
[27] Z. Tian, J.W. Davis, A.A. Haasz, J. Nucl. Mater. 399 (2010) 101–107.
[28] J.P. Roszell, J.W. Davis, A.A. Haasz, J. Nucl. Mater. 429 (2012).
[29] A.A. Haasz, J.W. Davis, M. Poon, et al., J. Nucl. Mater. 258–263 (1998) 889–895.
[30] W. Xiao, W.T. Geng, J. Nucl. Mat. 430 (2012) 132.
[31] K. Ohsawa, J. Goto, M. Yamakami, M. Yamaguchi, M. Yagi, Phys. Rev. B 82 (2010) 184117.
[32] K. Heinola, T. Ahlgren, K. Nordlund, J. Keinonen, Phys. Rev. B 82 (2010) 094102.